Journal of Sound and Vibration 328 (2009) 42–56

Contents lists available at ScienceDirect

Journal of Sound and Vibration

journal homepage: www.elsevier.com/locate/jsvi

Location optimization of a long T-shaped acoustic resonator array in noise control of enclosures

Ganghua Yu, Li Cheng *

Department of Mechanical Engineering, The Hong Kong Polytechnic University, Hung Hom, Kowloon, Hong Kong, SAR of China

ARTICLE INFO

Article history:
Received 5 November 2008
Received in revised form
18 June 2009
Accepted 25 July 2009
Handling Editor: L.G. Tham
Available online 19 August 2009

ABSTRACT

Acoustic resonators are widely used in various noise control applications. In the pursuit of better performance and broad band control, multiple resonators or a resonator array are usually needed. The interaction among resonators significantly impacts on the control performance and leads to the requirement for a systematic design tool to determine their locations. In this work, simulated annealing (SA) algorithm is employed to optimize the locations of a set of long T-shaped acoustic resonators (TARs) for noise control inside an enclosure. Multiple optimal configurations are shown to exist. The control performance in terms of sound pressure level reduction, however, seems to be independent of the initial resonator-locations. Optimal solutions obtained from the SA approach are shown to outperform other existing methods for a TAR array design. Numerical simulations are systematically verified by experiments. Optimal locations are then synthesized, leading to a set of criteria, applicable to the present configuration, to guide engineering applications. It is concluded that the proposed optimization approach provides a systematic and effective tool to optimize the locations of TARs in noise control inside enclosures.

1. Introduction

As noise control devices at low-frequencies, acoustic resonators, including Helmholtz resonator (HR) and their derivatives, have been widely investigated and used in many engineering applications [1–7]. Conventional HRs usually have bulbous bodies and long necks, which restricts their applications in small enclosures. Recently, long T-shaped acoustic resonators (TARs) emerged as a promising alternative to conventional HRs. A TAR consists of two mutually perpendicular tubes: a long closed-end tube and a short open-end one. Owing to its large aspect ratio, a TAR can be integrated into the host structure as a structural component, which relaxes the space requirement in the implementation. Since the work of Li and Vipperman [8], who structurally integrated TARs into an expendable launch vehicle (ELV) payload fairing, there has been a consistent interest in modeling, understanding and designing more effective TARs for given applications. In that effort, Li et al. [9] developed an acoustic coupled model to analyze the acoustic interaction between an enclosure and a TAR array for noise control inside an enclosure. It was observed, both numerically and experimentally, that the control performance is sensitive to the locations of the resonators. It was found that the optimal location for resonator installation may not be an arbitrary point in the anti-node surfaces of the targeted enclosure mode when considering multiple enclosure modes to achieve sound reduction within a chosen frequency band. Based on that model, a sequential design method (SDM) was proposed for determining the optimal locations of TARs [9]. In SDM, the optimal locations of individual

* Corresponding author.
E-mail address: mmlcheng@polyu.edu.hk (L. Cheng).

0022-460X/$ - see front matter Crown Copyright © 2009 Published by Elsevier Ltd. All rights reserved.
doi:10.1016/j.jsv.2009.07.026

resonators are determined sequentially. By doing so, the effects of the newly inserted resonators on the previous ones are neglected. Despite its apparent simplicity, SDM may fail when there exists a strong coupling among the resonators. This situation is very likely to occur when more resonators, or a resonator array, are needed to enlarge the frequency band of control [4,7,9]. Furthermore, SDM is a tedious and time-consuming method, which has to be executed manually at each step. In such cases, there is a need for a systematic optimization tool allowing the simultaneous consideration of multiple resonators to determine the installation location of each resonator for a given application. Unfortunately, such a tool does not yet exist for TAR design.

The main purpose of this study is to establish such a tool and to carry out numerical analyses and validations. Given an acoustic enclosure, the optimal locations of resonators will be systematically determined to achieve maximum sound pressure level (SPL) reduction within a frequency band centered at one chosen acoustic resonance. Confronting the problem of dealing with a large number of resonators and possible candidate locations, a suitable global optimization algorithm should be adopted. One option is the genetic algorithm (GA) which has been widely used in many cases such as the location optimizations of sensors or actuators [10–13], point masses on plate [14], and passive vibro-acoustic devices in a payload fairing [6], etc. Another option, which is the one to be adopted in the present work, is the simulated annealing (SA) algorithm. Based on a fully coupled model, this paper attempts to (1) develop a systematic procedure to determine the optimal locations of multiple resonators by taking into account the full coupling among them; (2) carry out systematic numerical and experimental analyses and establish design guidelines. Optimization results obtained using the present approach are also compared with those from SDM. Using selected configurations, experiments are conducted to verify the effectiveness of the proposed approach.

2. Theory

The system under investigation comprises a rigid-walled acoustic enclosure with a TAR array. A typical TAR is composed of three branches, which is shown in Fig. 1. Branches 2 and 3 are coaxial and branch 1 is perpendicular to them. The three branches 1–3 have physical lengths L_{B1}, L_{B2} and L_{B3}, and cross-sections S_1, S_2 and S_3, respectively. Variables related to "enclosure", "TAR" and "source" are denoted by the superscripts E, R, and S, respectively.

An acoustic interaction model between an enclosure and multiple resonators has been established in our previous work [9]. For the sake of completeness, this model is briefly reviewed hereafter. The SA approach is then introduced in more detail.

2.1. Acoustic interaction between an enclosure and a TAR array

An acoustic enclosure with acoustically rigid walls is considered. The acoustic pressure $p(\mathbf{r}, t)$ inside the enclosure is governed by the inhomogeneous wave equation [15]

$$\nabla^2 p(\mathbf{r},t) - \frac{1}{c^2}\ddot{p}(\mathbf{r},t) = -\rho_0 \dot{q}(t)\delta(\mathbf{r}-\mathbf{r}_0), \tag{1}$$

where $q(t)$ is the distribution of source volume velocity per unit volume; c the sound speed; and $\delta(\mathbf{r}-\mathbf{r}_0)$ the Dirac delta function. The primary sound field inside the enclosure is generated by a set of N harmonic sources with $q_1^S, q_2^S, \ldots, q_N^S$ centered at the points $\mathbf{r}_1^S, \mathbf{r}_2^S, \ldots, \mathbf{r}_N^S$; while M TARs with volume velocity distributions $q_1^R, q_2^R, \ldots, q_M^R$ located at the points $\mathbf{r}_1^R, \mathbf{r}_2^R, \ldots, \mathbf{r}_M^R$ (centers of the resonator aperture) form the secondary sound field. According to the definition of the acoustic impedance of a resonator Z, q^R is given by $q^R(t) = p(\mathbf{r}^R, t)/Z$, in which Z at the aperture of the resonator is computed by [8]

$$Z = \mathrm{i} z_0 \frac{1 - \frac{S_2}{S_1}\tan(kL_1)\tan(kL_2) - \frac{S_3}{S_1}\tan(kL_1)\tan(kL_3)}{S_1\tan(kL_1) + S_2\tan(kL_2) + S_3\tan(kL_3)},$$

where L_1, L_2 and L_3 are the effective lengths of the three branches, respectively. They can be computed by adding the corresponding end corrections to the physical lengths L_B. The end corrections for branches 1–3 are $8r_1/3\pi$, $1.5(8r_1/3\pi)$ and $1.5(8r_1/3\pi)$, respectively, in which r_1 is the internal radius of branch 1. Substituting q^R and q^S into Eq. (1) and expressing q^R

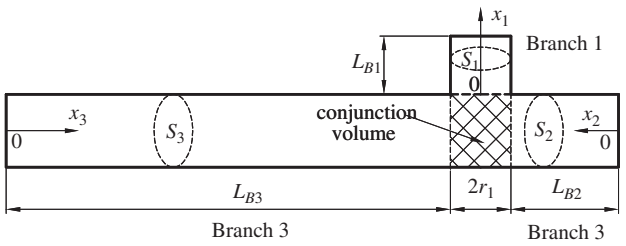

Fig. 1. A long T-shaped acoustic resonator.

by the acoustic impedance of TARs yield

$$\nabla^2 p(\mathbf{r},t) - \frac{1}{c^2}\ddot{p}(\mathbf{r},t) = -\rho_0\left[\sum_{m=1}^{M}\frac{\dot{p}(\mathbf{r},t)\delta(\mathbf{r}-\mathbf{r}_m^R)}{Z_m} + \sum_{n=1}^{N}\dot{q}_n^S(t)\delta(\mathbf{r}-\mathbf{r}_n^S)\right]. \tag{2}$$

$p(\mathbf{r}, t)$ can be decomposed on the basis of eigenfunctions of the enclosure: $p(\mathbf{r},t)=\sum_{j=1}^{J}\psi_j(t)\varphi_j(\mathbf{r})$, in which $\psi_j(t)$ is the time-dependent coefficient of the jth mode, $\varphi_j(\mathbf{r})$ is the jth eigenfunction and J is the maximum number of the truncated mode series. Substituting this modal expansion into Eq. (2) and applying orthogonality properties of the eigenfunctions yield a discrete acoustic equation

$$\ddot{\psi}_j(t) + (\gamma_j^E)^2\psi_j(t) = \frac{cz_0}{V^E}\sum_{m=1}^{M}\sum_{h=1}^{J}\frac{\varphi_j(\mathbf{r}_m^R)\varphi_h(\mathbf{r}_m^R)}{Z_m\Lambda_j}\dot{\psi}_h(t) + \frac{cz_0}{V^E}\sum_{n=1}^{N}\frac{\tilde{\varphi}_j(\mathbf{r}_n^S)}{\Lambda_j}\dot{q}_n^S(t), \tag{3}$$

where $z_0=\rho_0 c$; z_0 is the characteristic impedance of the fluid; V^E the volume of the enclosure; Λ_j the mode normalization factor of the enclosure given by $\Lambda_j=\int_{V^E}[\varphi_j(\mathbf{r})]^2\,\mathrm{d}V/V^E$; $\tilde{\varphi}_j(\mathbf{r}_n^S)$ the averaged $\varphi_j(\mathbf{r}_n^S)$ over the volume of the nth primary source; γ_j^E the jth eigenvalue of the enclosures expressed as $\gamma_j^E=\omega_j^E+\mathrm{i}C_j^E$, in which the real part is the angular frequency and the imaginary part is an equivalent *ad hoc* damping coefficient.

Assuming all time dependent variables are harmonic, i.e. $\psi_j(t)=P_h\mathrm{e}^{\mathrm{i}\omega t}$ and $q_n^S=\tilde{Q}_n^S\mathrm{e}^{\mathrm{i}\omega t}$, Eq. (3) can be rewritten as

$$[\omega^2-(\gamma_j^E)^2]P_j + \frac{\mathrm{i}\omega cz_0}{V^E}\sum_{m=1}^{M}\sum_{h=1}^{J}\frac{\varphi_j(\mathbf{r}_m^R)\varphi_h(\mathbf{r}_m^R)}{Z_m\Lambda_j}P_h = -\frac{\mathrm{i}\omega cz_0}{V^E}\sum_{n=1}^{N}\frac{\tilde{\varphi}_j(\mathbf{r}_n^S)}{\Lambda_j}(\tilde{Q}_n^S), \tag{4}$$

where $\tilde{Q}^S$ is the volume velocity source strength of the primary source located at $\mathbf{r}^S$.

Eq. (4) shows that, given the resonator impedance, the resonator locations, through $\varphi(\mathbf{r}^R)$, play an important role in determining the effect of resonators. As illustrated for a single resonator [9], the insertion of the resonator creates two new peaks as shown in Fig. 2, which are loosely called coupled peaks hereafter. The amplitudes of these coupled peaks are sensitive to the property of the resonator as well as its location. If the control performance needs to be evaluated in a broad frequency band, these coupled peaks should be meticulously controlled. In the case of multiple resonators, the amplitudes of the coupled peaks further depend on other resonators because of their interaction as shown by Eq. (4). This effect can be demonstrated using a simple case, i.e. the interaction between two resonators and a single enclosure mode. By using a single resonator, R1, to target the jth enclosure mode, the modal response $(P_1)_j$ of the enclosure can be obtained from Eq. (4) as

$$[\omega^2-(\gamma_j^E)^2](P_1)_j + \frac{\mathrm{i}\omega cz_0}{V^E}\frac{\varphi_j^2(\mathbf{r}_1^R)}{Z_1\Lambda_j}(P_1)_j = -\frac{\mathrm{i}\omega cz_0}{V^E}\sum_{n=1}^{N}\frac{\tilde{\varphi}_j(\mathbf{r}_n^S)}{\Lambda_j}(\tilde{Q}_n^S). \tag{5a}$$

Upon inserting a second resonator R2, the modal response $(P_2)_j$ is given by

$$[\omega^2-(\gamma_j^E)^2](P_2)_j + \frac{\mathrm{i}\omega cz_0}{V^E}\left[\frac{\varphi_j^2(\mathbf{r}_1^R)}{Z_1\Lambda_j}+\frac{\varphi_j^2(\mathbf{r}_2^R)}{Z_2\Lambda_j}\right](P_2)_j = -\frac{\mathrm{i}\omega cz_0}{V^E}\sum_{n=1}^{N}\frac{\tilde{\varphi}_j(\mathbf{r}_n^S)}{\Lambda_j}(\tilde{Q}_n^S). \tag{5b}$$

Equalizing the left hand sides of Eqs. (5a) and (5b), the ratio of P_2 to P_1 can be expressed as

$$\frac{(P_2)_j}{(P_1)_j} = 1 - \frac{\varphi_j^2(\mathbf{r}_2^R)}{-\mathrm{i}Z_2\dfrac{\Lambda_j V^E}{\omega cz_0}[\omega^2-(\gamma_j^E)^2] + \dfrac{Z_2}{Z_1}\varphi_j^2(\mathbf{r}_1^R)+\varphi_j^2(\mathbf{r}_2^R)}. \tag{6}$$

It can be observed from Eq. (6) that when the resonance frequency of R2 is very different from that of R1, a large impedance of R2 results, which makes the second item on the right hand side of this equation much less than one. This means the pressure change induced by R2 is small and the interaction between two resonators can be neglected. However, when R2 is used to control one of the coupled modes produced by R1, for example the lower one, R2 can induce two newly emerged peaks very close to the resonance frequency of R1, as shown in Fig. 2. According to Eq. (6), the amplitudes of these two

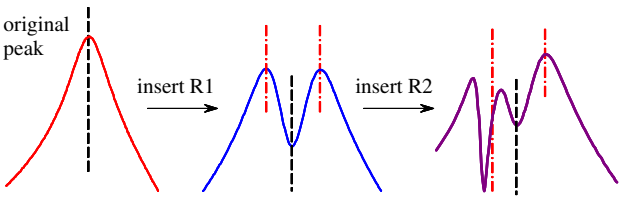

Fig. 2. Coupled peaks induced by the insertion of resonators.

peaks are affected by the resistances of both resonators. Therefore, the two resonators influence each other and the attenuation of SPLs in the frequency band of interest depends on the characteristics of both resonators.

One can suspect that a similar phenomenon also occurs when the resonators are acoustically coupled to the multiple enclosure modes. In that case, apart from the impedance of the resonators, the locations of R1 and R2 also become the decisive parameters to affect the overall control performance. A change in the location of either resonator can alter the amplitudes of all resonance peaks induced by R1 and R2. Good control in the frequency band of interest can only be achieved through a careful optimization of the locations of these two resonators. It also means that the multiple resonators should be considered simultaneously during the optimization process.

2.2. Objective function and optimization procedure

It is known that the insertion of acoustic resonators can induce coupled peaks [1]. In order to achieve an overall control in the vicinity of the targeted frequency, the objective function is defined as the minimization of the maximum SPL in a frequency band around the targeted frequency [16]:

$$\begin{cases} \min & \text{obj} = \max\limits_{\omega\in[\omega_1,\omega_2]}[\hat{p}(\omega)] \\ \text{subject to} & \mathbf{r}_1^R, \mathbf{r}_2^R, \ldots, \mathbf{r}_M^R, \end{cases} \tag{7}$$

where obj is the raw objective function value and $\hat{p}$ is the amplitude of the acoustic pressure. The SPL is either calculated at a single location or averaged in a concerned volume. The optimal resonator locations are determined by the SA algorithm.

SA was early explored by Kirkpatrick et al. [17] to solve the combinatorial optimization problems, such as the computer design and traveling salesmen problem. It is implemented by Metropolis Monte Carlo techniques and has analogous procedures as material annealing in the thermodynamics field. In physical annealing process, initially material is under the disordered state at a high temperature. When the temperature is reduced slowly, the long enough annealing time can allow thermal equilibrium to be approximately reached at each cooling stage. Eventually, material is crystallized to form crystalline structure with the lowest energy level. If the initial temperature of the system is too low or the cooling speed is too rapid, amorphous structure with a higher energy level may occur instead. By analogy, SA starts at a high initial temperature T_0. At each temperature T, enough iterative searches are performed to seek the minimum of the objective function value. In iterations, the potential solution is accepted when a random value uniformly distributed in [0, 1] is less than the Metropolis probability M_p given by

$$M_p = \exp(-\Delta E/T),$$

where ΔE is the difference between the current value of the objective function and old one. The new solution is randomly generated based on the previous accepted one. After finishing one annealing stage, the new temperature is calculated by $T_{\text{new}} = \gamma_T \cdot T$, in which γ_T is the temperature reduction coefficient. With T gradually decreasing, the optimization process is terminated under a certain criterion at the end and the optimal solution is obtained.

Later, the application of SA was extended from discrete problems [17–19] to continuous problems by different methods [20–22]. The comparison among these methods made by Goffe et al. [23] concluded that the approach suggested by Corana et al. [22] was a more robust and easier one. Because the locations of TARs vary continuously inside the enclosure, this paper will use the modified SA [22] to conduct the optimization. According to Corana's method [22], the location of each resonator is adjusted along each direction in turn by

$$x_j^{new} = x_j + \mu(s_m)_h \mathbf{e}_h,$$

where x_j is the jth accepted configuration of the real-valued locations of the TAR array; x_j^{new} the new generated configuration to be accepted or rejected; μ the random number uniformly distributed in $[-11]$; $\mathbf{e}_h$ the direction vector associated to the hth components in x; and $(s_m)_h$ the step adjusting factor along the same direction in mth step, which is computed by the former one as

$$(s_m)_h = (A_f)_h \cdot (s_{m-1})_h,$$

where A_f is the amplifying factor. In SA, this factor controls the rate of the accepted to the rejected location adjustments of the TAR array at each adjustment cycle. A possible choice is to maintain the average rate to be 1:1 as Corana did [22], who defined the amplifying factor as

$$(A_f)_h = \begin{cases} 1 + \alpha_h \dfrac{n_h/N_s - 0.6}{0.4}, & n_h > 0.6N_s, \\ \dfrac{1}{\left(1 + \alpha_h \dfrac{0.4 - n_h/N_s}{0.4}\right)}, & n_h < 0.4N_s, \\ 1, & \text{others}, \end{cases} \tag{8}$$

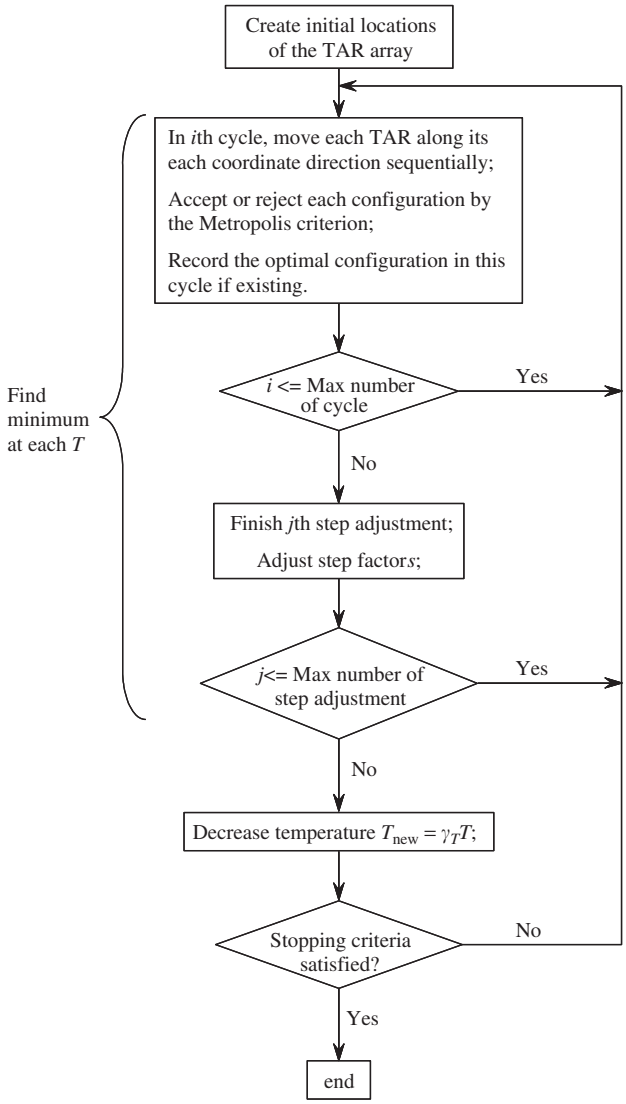

Fig. 3. Flow chart showing the SA process.

where N_s is the allowed maximum number of the successive adjustments of the locations of the TAR array, n_h is the number of the accepted adjustments in hth direction in the adjustment cycle and α_h is a factor. By this step adjustment approach and the Metropolis acceptance criterion, SA can therefore perform the optimization of the locations for the TAR array. Initially large step length is preferred in SA to build up a rough view of the effect of the locations of the TAR array on its performance. As the temperature gradually falls, the moving step length of resonators decreases and the potential installation locations of the TAR array shrink from the whole enclosure surfaces to some most promising areas. The entire optimization process is illustrated in Fig. 3.

SA has several advantages as described in [16,21,22]. The most appealing one for the current case is its ability to identify the corner solutions because the enclosure used in this paper has a rectangular shape and its corners are possibly the optimal locations of some individuals in the TAR array. This will be observed in the following simulations.

3. Simulations and experimental validation

The system setup is shown in Fig. 4, in which a right parallelepiped enclosure with dimensions $L_x = 976.0$ mm, $L_y = 695.0$ mm, and $L_z = 1188.0$ mm was used in both numerical simulations and experiments. The enclosure to be tested was composed of six plywood boards, 2-in thick each. Five of them were bolted together to form a cavity and one of them was made removable as a cover. To prevent any possible leakage, sound-proof strips were used in the connecting surfaces

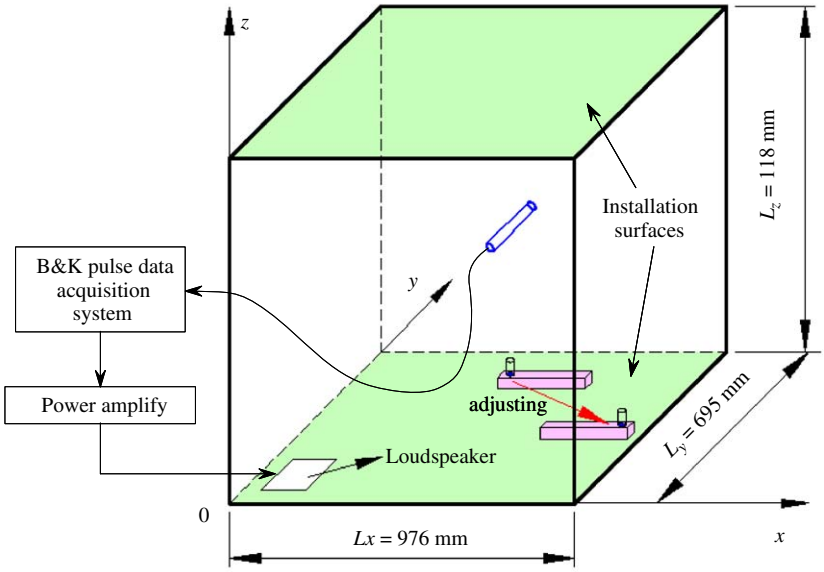

Fig. 4. System used in simulations and experiments.

Table 1
Computed natural frequencies and measured *Q*-factors of the enclosure.

Index	Mode number (*lmn*)	Natural frequency (Hz)	*Q*-factor
1	000	0	–
2	001	145	32
3	100	176.5	42
4	101	228.4	44
5	010	247.8	46
6	011	287.1	84
7	002	290	42
8	110	304.3	51
9	111	337	79
10	102	337	65
11	200	353	80
12	012	381.5	60
13	201	381.6	45
–	–	>400.0	45

between the bolted boards and the removable board and silicon gel was also used at the connection corners of the bolted boards. A square hole of 100.0 mm × 100.0 mm was cut at (100.0, 59.0) mm in the cover through which a loudspeaker was installed to create a primary sound field in the enclosure. A Brüel & Kjær pulse system was used to generate the white noise signal for the loudspeaker and collect the microphone response. The position of the microphone for getting the modal characteristics of the enclosure was carefully adjusted. In the case of well separated mode, the resonance frequency and the *Q*-factor of particular enclosure mode were measured by locating the microphone at the anti-node point. Method for choosing such locations and possible effects have been well documented in Ref. [24]. In the case of well-coupled modes with very close resonance frequencies, the microphone position was varied so that their responses can be separated. Using this method, the *Q*-factors for the present enclosure were measured, respectively, and are listed in Table 1. The *Q*-factors for higher-order modes (with natural frequencies >400 Hz) were assumed to be 45, which is the same as the measured value for the mode (2, 0, 1). Given the ambient temperature of 20 °C and the humidity of 90 percent, the sound speed was determined as 344.5 m/s. The air density ρ_0 was 1.205 kg/m^3.

In simulations, 216 enclosure modes were used, as determined by a convergence study. The eigenfunctions $\varphi_j(\mathbf{r}^R)$ of the enclosure, having thermalviscous boundary conditions, were given in Ref. [4]. The calculated natural frequencies of the first 13 modes are tabulated in Table 1. Notice that due to the difficulty in determining the volume velocity source strength $\tilde{Q}^S$ for primary sources used in experiments, the dimensionless modal response $P_i/(iz_0\tilde{Q}^S/kV^E)$ was solved and used to calculate the SPL in simulations. Therefore, the predicted SPL cannot be directly compared with the measured SPL. Instead,

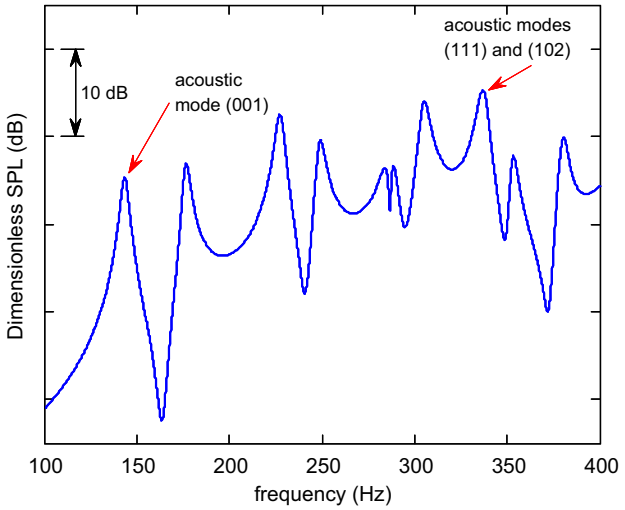

Fig. 5. Predicted baseline SPL curve at (816, 70, 1028) mm.

the comparison will focus on the general trends and the control performance of resonators. In the SA process, the SPL at (816, 70, 1028) mm near one corner of the enclosure was chosen as the control target. The predicted baseline SPL without the resonator is shown in Fig. 5, in which major peaks correspond to the enclosure modes listed in Table 1.

3.1. Searching strategy

Optimization can be carried out by the following two different search strategies: volume searching and surface searching. Volume searching allows exploration of the entire volume of the enclosure. It is computational efficient since the locations of the TARs can be continuously varied. However, solutions may converge at local optimum. On the contrary, surface searching confines the searching space to the pre-selected surfaces. It is more physical and can be guided by Eq. (4), which shows that resonators need to be located in the anti-node surfaces in order to maximize the control effect. This definitely decreases the probability of being trapped by local optimum. Although surface searching reduces the exploration space compared with volume searching, it is more computational intensive since intermediate solutions may jump from one surface to another in a discontinuous manner. In the present case, candidate locations for surface searching are the walls of the enclosure. Constrained by the installation of the TAR inside the enclosure, the closest distance between the TAR orifice and any wall surface of the enclosure is 60.0 mm (sum of the length of branch 1 and the height of branch 2 or 3). For example, for the enclosure mode (0, 0, 1), the two searching surfaces are $z = 60$ mm and $z = L_z - 60$ mm.

3.2. Determination of parameters in SA algorithm

Successful SA optimization requires slow annealing from a high initial temperature. However, an excessively high initial temperature or slow annealing significantly leads to the excessive computation time. To find the suitable SA parameters to be used in the present physical problem, the effect of the initial temperature T_0 and the temperature reduction coefficient γ_T are firstly examined using one resonator to control the mode (0, 0, 1) at 145 Hz. Hereafter, the resonator is labeled using a "TAR_" and an integer indicting the resonator's Helmholtz frequency, such as TAR_145 for the above one. According to the numerical simulation, the optimal location for TAR_145 was at the corner (976, 0, 1128) mm, as shown in Fig. 6(a).

In simulations, the control performance of TARs at mode (0, 0, 1) was evaluated in a frequency band [130,160] Hz. T_0 was varied from 0.5 to 5 with a step of 0.5 when $\gamma_T = 0.85$, 0.90, 0.95, 0.98 and 0.99, respectively. For each combination of T_0 and γ_T, 10 runs of SA process with different initial locations of TAR_145 were executed. These 10 initial locations remain the same throughout the tested combinations. The comparisons among these combinations suggest that ($T_0 = 2$, $\gamma_T = 0.98$) is the best combination. It led all runs to converge at the global optimal location as shown in Fig. 6(b); any further decrease of either T_0 or γ_T deteriorated the performance of SA, such as the two examples shown in Fig. 6(c) and (d), corresponding to ($T_0 = 2$, $\gamma_T = 0.95$) and ($T_0 = 1$, $\gamma_T = 0.98$), respectively. Therefore, ($T_0 = 2$, $\gamma_T = 0.98$) will be used in the following simulations. Fig. 6(b) also shows the strong ability of SA in identifying the corner solution when its parameters are properly chosen.

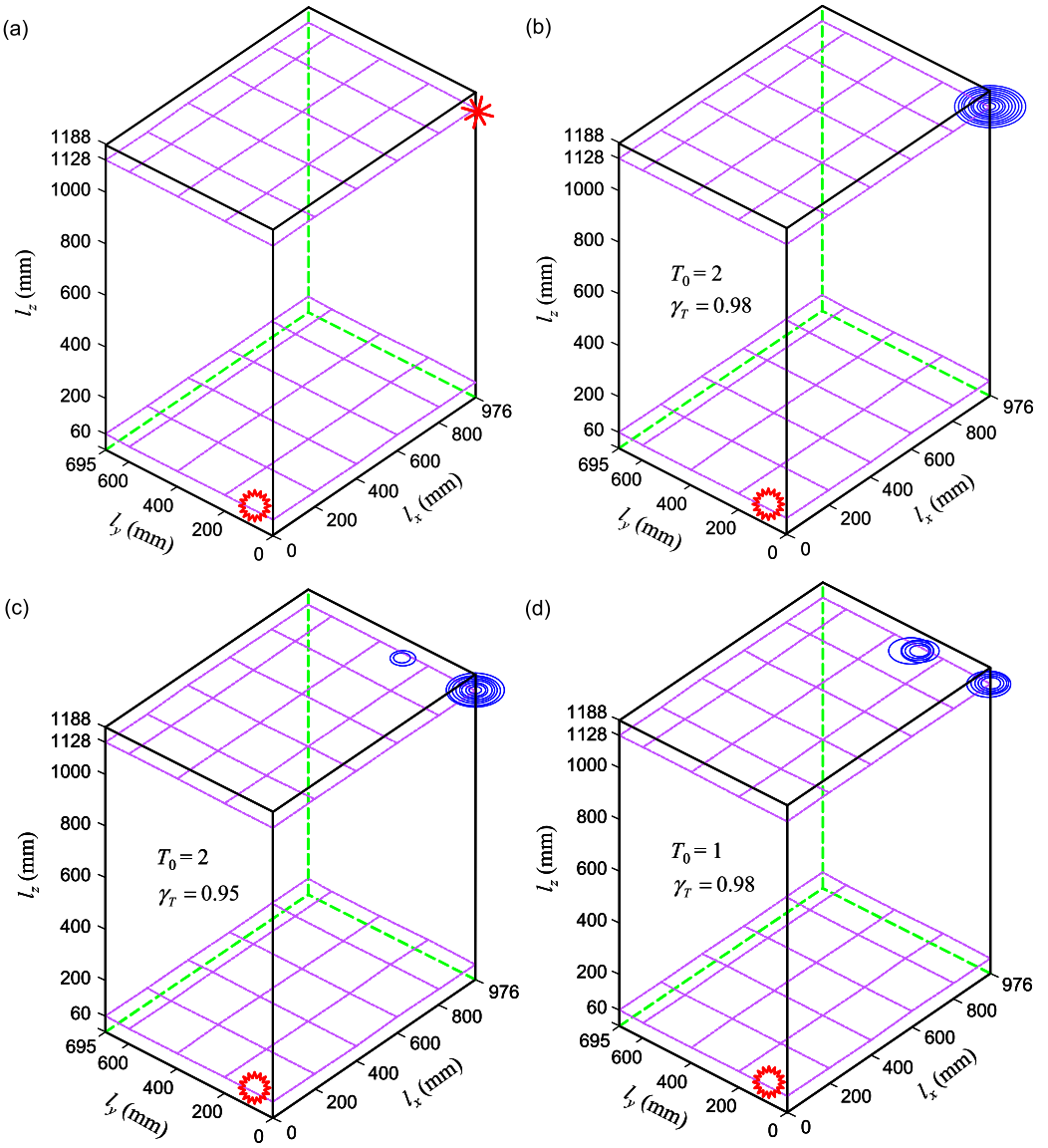

Fig. 6. (a) The best location of TAR_145 ✱; location distribution of TAR_145: (b) $T_0 = 2$, $\gamma_T = 0.98$; (c) $T_0 = 2$, $\gamma_T = 0.95$; (d) $T_0 = 1$, $\gamma_T = 0.98$.

Table 2
Parameters of TARs.

Name of TAR	Resonance frequency (Hz)	Branch 1 (circular tube)		Branches 2 and 3 (square tube)		
		Diameter (mm)	L_{B1} (mm)	Cross-section (mm)	L_{B2} (mm)	L_{B3} (mm)
TAR_145	145	21.0	30.0	29.5 × 29.5	20.0	482.4
TAR_142	142					495.0
TAR_147	148					470.4
TAR_138	138					510.8
TAR_143	143					490.8
TAR_146	146					479.2
TAR_150	150					463.4
TAR_337	337					142.6
TAR_329	329					148.6
TAR_345	345					136.6

3.3. Location optimization for multiple TARs and experimental verification

3.3.1. Control of well separated mode

In this section, the enclosure mode (0, 0, 1) was chosen as the control mode. After using TAR_145, two new coupled peaks appeared at 142 and 147 Hz. Another two TARs were designed to control these two coupled peaks, respectively. Parameters of three TARs are tabulated in Table 2. The resonance frequency of the TAR was adjusted by varying the length of branch 3.

Due to the stochastic nature of the SA algorithm, several runs of the optimization process were conducted to evaluate its overall performance. Since the initial locations were randomly generated in each run, this also allows examining the effect of the initial resonator locations on the optimization outcome. To this end, 15 runs were conducted with randomly generated starting locations for three TARs. Results are tabulated in Table 3, in which a prefix "Surf-" put before the ranking number stands for surface searching.

Table 3 shows that, despite the noticeable differences between different runs, the final optimal locations of three TARs formed several clusters and concentrated within a few areas. Obviously, the outcome is not unique. The complex interaction between the multiple resonators and the multiple modes of the enclosure allows the multiple optimal configurations of the TAR locations. The SPL reductions corresponding to the different optimal locations, however, were

Table 3
Optimal locations of three TARs targeting the peak at 145 Hz.

Group name	Performance ranking	SPL reduction (dB)	Optimal locations of TARs (mm)		
			TAR_145	TAR_142	TAR_147
Surf-1	1	6.8	(907, 557, 1128)	(975, 693, 1128)	(740, 115, 1128)
Surf-2	2	6.8	(893, 559, 1128)	(975, 695, 1128)	(169, 209, 60)
Surf-3	3	6.8	(908, 557, 1128)	(974, 691, 1128)	(727, 101, 1128)
Surf-4	4	6.8	(894, 559, 1128)	(975, 695, 1128)	(146, 223, 60)
Surf-5	5	6.8	(895, 560, 1128)	(975, 695, 1128)	(186, 195, 60)
Surf-6	6	6.8	(891, 562, 1128)	(971, 691, 1128)	(172, 207, 60)
Surf-7	7	6.8	(889, 563, 1128)	(976, 686, 1128)	(148, 222, 060)
Surf-8	8	6.8	(906, 559, 1128)	(976, 695, 1128)	(768, 136, 1128)
Surf-9	9	6.8	(896, 558, 1128)	(975, 695, 1128)	(177, 203, 60)
Surf-10	10	6.8	(893, 561, 1128)	(976, 695, 1128)	(193, 188, 60)
Surf-11	11	6.8	(896, 561, 1128)	(975, 695, 1128)	(244, 125, 60)
Surf-12	12	6.8	(896, 561, 1128)	(976, 695, 1128)	(254, 107, 60)
Surf-13	13	6.8	(900, 559, 1128)	(976, 695, 1128)	(223, 155, 60)
Surf-14	14	6.8	(901, 559, 1128)	(973, 694, 1128)	(258, 94, 60)
Surf-15	15	6.8	(068, 579, 60)	(0, 695, 60)	(818, 177, 1128)

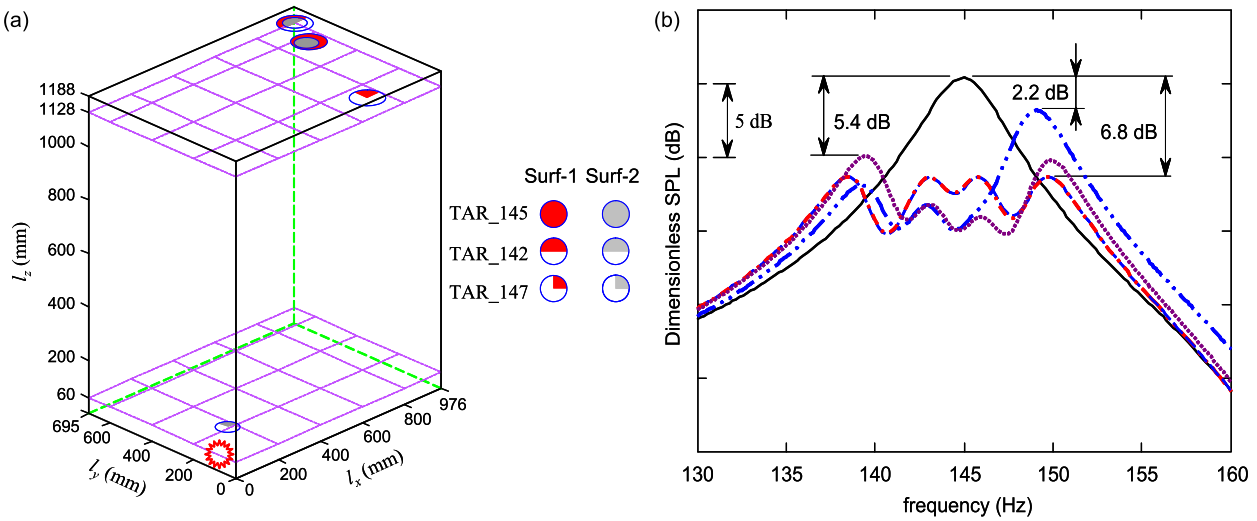

Fig. 7. Numerical results showing the effect of the resonator locations with three TARs for the peak control at 145 Hz. (a) Locations of three TARs in Suf-1 and Surf-2 configurations; (b) predicted SPL curves at (816, 70, 1028) mm: — without resonator; —·— with TARs in Surf-1 configuration; —— with TARs in Surf-2 configuration; · · · with TARs at the first group of arbitrary locations; —· ·— with TARs at the second group of arbitrary locations.

Table 4
Two groups of arbitrary locations of three TARs targeting the peak at 145 Hz.

Group no.	Locations of TARs (mm)		
	TAR_145	TAR_142	TAR_147
Gr. 1	(676, 265, 60)	(92, 452, 1128)	(961, 22, 60)
Gr. 2	(884, 320, 1128)	(131, 463, 60)	(461, 166, 1128)

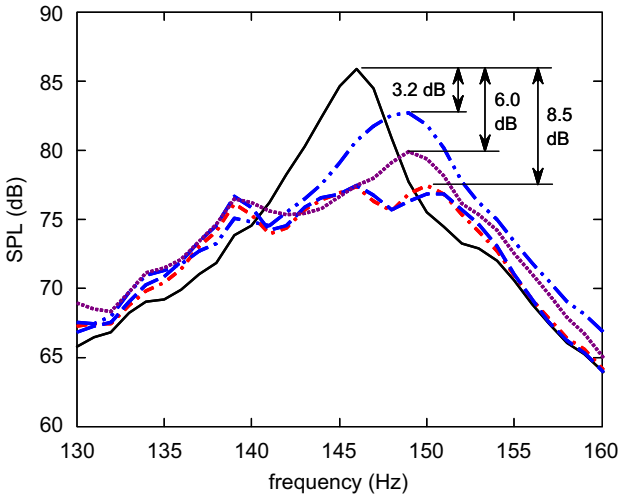

Fig. 8. Experimental results showing the effect of the resonator locations with three TARs for the peak control at 145 Hz. Measured SPL curves at (816, 70, 1028) mm: — without resonator; — · — with TARs in Surf-1 configuration; —— with TARs in Surf-2 configuration; · · · with TARs at the first group of arbitrary locations; —· ·— with TARs at the second group of arbitrary locations.

basically the same (difference can only be detected a few digits after the decimal in SPL values). This suggests that the SPL reduction resulted from the SA optimization process is independent of the initial locations of the TAR array since different initial locations were used in different runs.

The first two groups (Surf-1 and Surf-2) are shown in Fig. 7(a). Corresponding SPL curves are presented and compared to another two cases when TARs were located at two groups of arbitrarily selected locations listed in Table 4. Fig. 7(b) shows that 5.4 and 2.2 dB reductions in SPL were achieved in the chosen band by the two arbitrary groups, respectively. For both optimized groups, a better performance with 6.8 dB reduction was achieved in the same frequency band and the predicted SPL curves for these two cases were almost identical.

Experimental measurements were conducted to validate above predicted optimal locations of the TAR array. Similar as in simulations, the enclosure mode (0, 0, 1) was chosen as the targeted mode at the measured natural frequency of 145 Hz. A Brüel & Kjær Type 4189 $\frac{1}{2}$ in microphone was installed at (816, 70, 1028) mm to collect the SPL inside the enclosure. The Surf-1 and Surf-2 from SA and above two groups of arbitrary locations were tested in experiments. Fig. 8 shows the measured SPL curves for these four installation cases and their counterpart without resonator. It can be seen that the two arbitrary groups led to 6 and 3.2 dB reductions in SPL in the band of interest, respectively. The two optimized cases, Surf-1 and Surf-2, both resulted in 8.5 dB reduction in the same frequency band. Comparing with the predicted results in Fig. 7(b), the same variation tendency is observed.

It is relevant to note that, prior to the validation, possible effect of the volume change due to the insertion of the resonators were experimentally assessed. Measurements were conducted when the orifices of all TARs were closed. The SPL was compared with the one without resonators. By testing a series of resonator locations, it was observed that the insertion of TARs with closed orifices only brought about very slight changes in SPL, due to the very small volume of the resonators compared with that of the enclosure. Since the present work is focused on the control within a chosen bandwidth, not at one particular frequency, the slight changes due to the insertion of the resonators are deemed to be negligible.

3.3.2. Control at closely spaced modes

Control of modes (1, 1, 1) and (1, 0, 2) was examined in this section. The characteristic of these two modes is that they have very close or even identical natural frequencies and therefore strongly coupled together. Simulation predicted 337 Hz for the resonance frequencies of both modes, whilst measurement gave 334 Hz. Due to the closeness between these two modes, the predicted SPL levels around their natural frequencies are very sensitive to the enclosure parameters. These

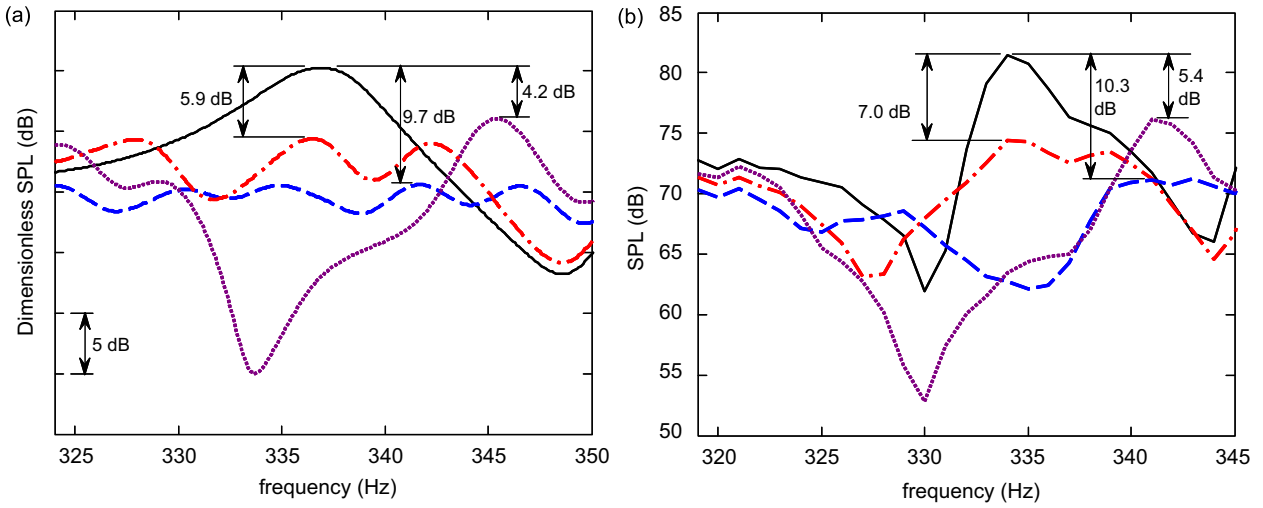

Fig. 9. Numerical and experimental results showing the effect of the resonator locations with four TARs for the peak control at 337 Hz. (a) Predicted SPL curves: — without resonator; — · — with TAR_337 at optimal location; —— with four TARs at optimal locations; · · · with TARs at a group of arbitrary locations; (b) measured SPL curves: — without resonator; — · — with TAR_334 at optimal location; —— with four TARs at optimal locations; · · · with TARs at a group of arbitrary locations.

Table 5
Locations of four TARs targeting the peak at 337 Hz.

	Locations of TARs (mm)			
	TAR_337 (1st)	TAR_329	TAR_337 (2nd)	TAR_345
Optimal case	(916, 546, 106)	(166, 522, 60)	(60, 177, 335)	(222, 60, 474)
Arbitrary case	(916, 546, 106)	(166, 522, 60)	(60, 177, 335)	(40, 665, 1128)

parameters, therefore, have to be properly determined from the measured baseline data as specified in the first paragraph of Section 3.

In numerical simulations, a TAR was firstly designed to target the peak at 337 Hz in SPL curve. This gave the optimal location at (60, 520, 1180) mm with the predicted SPL curve shown in Fig. 9(a) by a dot-dashed line. A 5.9 dB reduction was achieved in the band [320,350] Hz. Three new coupled peaks were also observed, corresponding to three new coupled modes in the enclosure–resonator coupling system. The natural frequencies of these coupled modes can be well predicted from the theoretical model established by following the procedure used in Ref. [7], which were 329.4, 337.1 and 345 Hz, respectively. To further control these coupled modes, another three TARs, i.e. TAR_329, TAR_337 and TAR_345, were then designed. The parameters of all four TARs are listed in Table 2. Using SA, the locations of all TARs were simultaneously optimized and one group of optimal results is listed in Table 5. The corresponding SPL curve is plotted in Fig. 9(a) by a dashed line. It can be seen that eventually a 9.7 dB reduction was obtained in the frequency band of interest. For comparison purpose, the SPL was also computed after moving TAR_345 to a corner of the enclosure (40, 665, 1128) mm with other TARs remaining at their optimal locations. This formed a so-called "arbitrary location" case. A 4.2 dB SPL reduction was obtained as shown in Fig. 9(a), which is much lower than that achieved by the optimal case.

TARs were then fabricated and tuned for experimental validations. The measured SPL curves with and without TARs are shown in Fig. 9(b). It is noticed that the measured baseline curve (before resonators were installed) undergoes similar variations as the predicted one in Fig. 9(a) except the dip around 330 Hz. The installation of TAR_334 at its optimal location provided a 7.0 dB SPL reduction in experiment. When four TARs were used, the optimal installation case and the arbitrary one resulted in SPL reductions of 10.3 and 5.4 dB, respectively. Compared to the predicted results shown in Fig. 9(a), a strong resemblance between simulations and experiments can be observed. Local discrepancies, especially in the region around 330 Hz, are due to the differences between the simulation model and the test rig observed previously in the baseline SPL curves.

As expected, the two control examples using TARs at different enclosure modes both show the good agreement between simulations and experiments, testifying the validity of the proposed optimization approach. It should be pointed out that the above validation also testifies the effectiveness of the surface searching strategy. It should be cautioned, however, that the efficiency of the surface searching method decreases with the increase of the number of TARs, since the number of

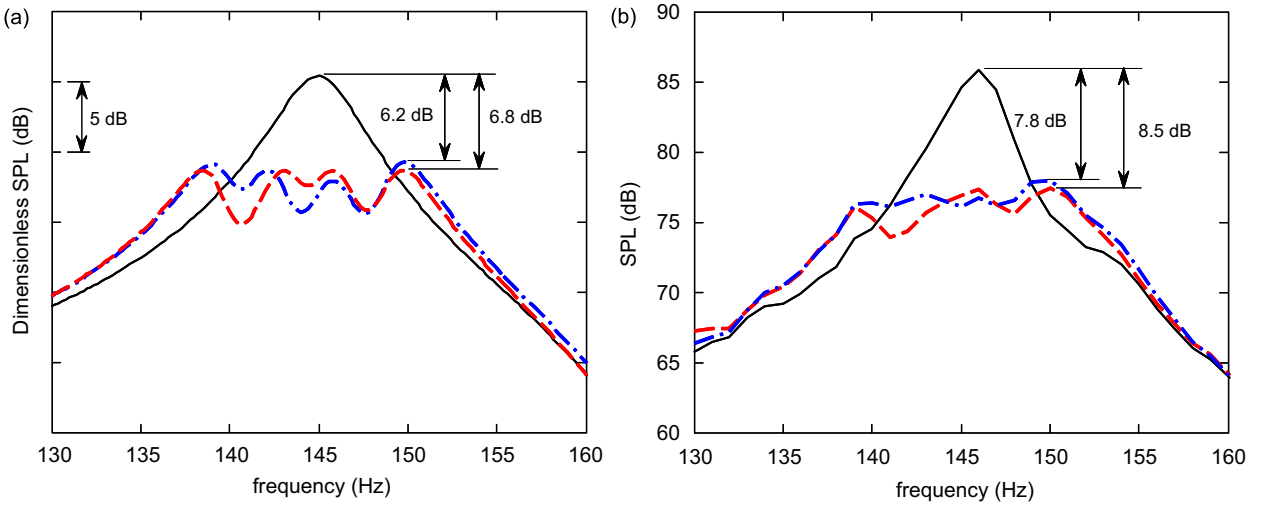

Fig. 10. Numerical and experimental comparisons on SA and SDM. (a) Predicted SPL curves: — without resonator; —— with TARs in Surf-1 configuration; —·— with TARs in the configuration from SDM; (b) measured SPL curves: — without resonator; —— with TARs in Surf-1 configuration; —·— with TARs in the configuration from SDM.

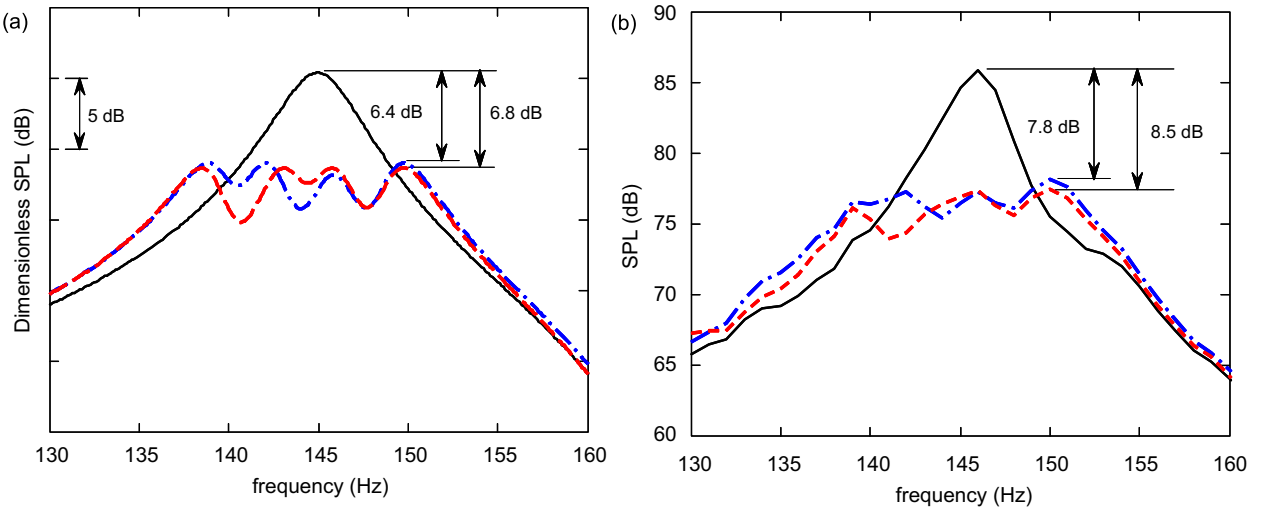

Fig. 11. Numerical and experimental comparisons on SA and SA+SDM. (a) Predicted SPL curves: — without resonator; —— with TARs in Surf-1 configuration; —·— with TARs in the configuration from SA+SDM; (b) measured SPL curves: — without resonator; —— with TARs in Surf-1 configuration; —·— with TARs in the configuration from SA+SDM.

combinations of the possible searching surfaces dramatically increases. When that happens, surface searching becomes very time-consuming.

3.4. Comparison with SDM optimization approach

By SDM, the optimal locations of TAR_145, TAR_142 and TAR_147 were determined one by one as (976, 0, 60), (920, 660, 60), and (680, 220, 1128) mm, respectively. The solution thus obtained is compared to the Surf-1 obtained from SA in Section 3.3.1. It is noticed that the optimal locations obtained from two optimization approaches are much different. The predicted SPL curves for these two installation cases are shown in Fig. 10(a). The SA solution provided 0.6 dB higher reduction in SPL than the one from SDM in the frequency band of interest. This observation was again verified by the experimental results as shown in Fig. 10(b), in which 0.7 dB further reduction was experimentally achieved using the optimized configuration from SA.

Due to the long annealing time required by SA process, it was considered to combine the SA process with SDM. SDM was used to determine the optimal location of TAR_145 whilst those of other two TARs were optimized by the SA approach. Using this hybrid procedure, the locations of TAR_145, TAR_142 and TAR_147 were determined as (976, 0, 60), (938, 6, 60) and (711, 193, 60) mm, respectively. This configuration is compared, both numerically and experimentally, with the Surf-1 case, in Fig. 11(a) and (b), respectively. Compared with the SA solution, the combined hybrid approach resulted in 0.4 and 0.7 dB less reductions in simulations and experiments, respectively. This deficiency in terms of SPL reduction is apparently due to the negligence of the coupling between TAR_145 and the two other TARs, which has previously been pointed out in Section 2.1.

3.5. Criteria for engineering application

Results presented before show that the SA optimization procedure results in multiple TAR locations which form slightly scattered clusters within a few areas. The so-called optimal locations can therefore be better described in terms of optimal patches within which the deviation between the actual SPL reductions and the optimized maximum can be caped to a prescribed value. This is also useful from a practical point of view, since it is not always possible to accurately install resonators at the precise optimal locations due to the installation error or even the space limitation. In that case, possible deterioration in SPL reduction should also be evaluated. Using the Surf-1 configuration in Section 3.3.1, each resonator was moved around in the vicinity of its optimal location. When moving one resonator, the other two were being fixed to their optimal locations. This gives Fig. 12(a)–(c), showing the contour of SPL reduction when moving TAR_145, TAR_142 and TAR_147, respectively. It was observed that, when a resonator is installed within a certain distance from its optimal location, the SPL reduction can be kept close to the optimal value. Typically, within a circle of $\lambda/50$ in radius, where λ is the acoustic wavelength, the deterioration in SPL reduction was below 0.5 dB in the present case. Within a circle of $\lambda/30$, the

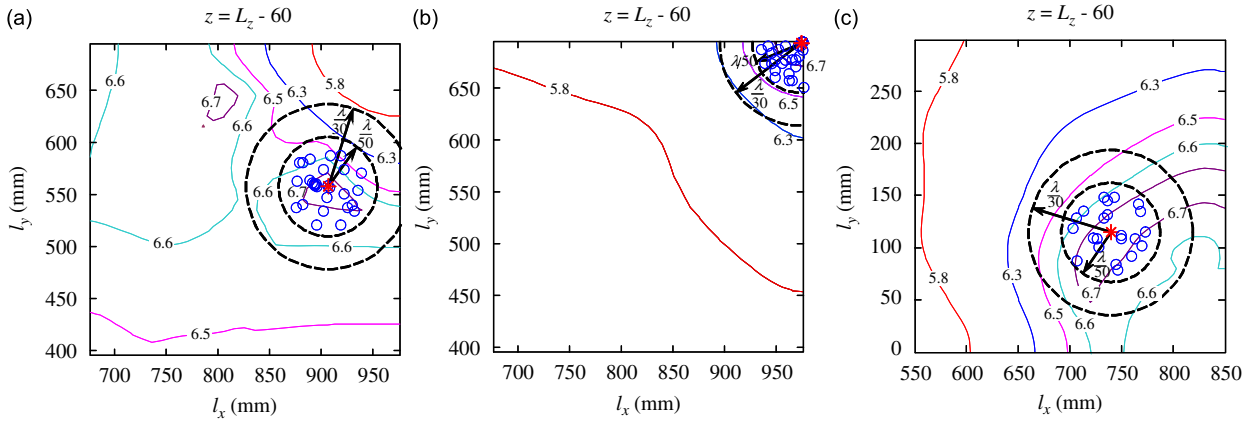

Fig. 12. Deviation criteria of the optimal locations of TARs in Surf-1 configuration: (a) deviation of TAR_145; (b) deviation of TAR_142; (c) deviation of TAR_147.

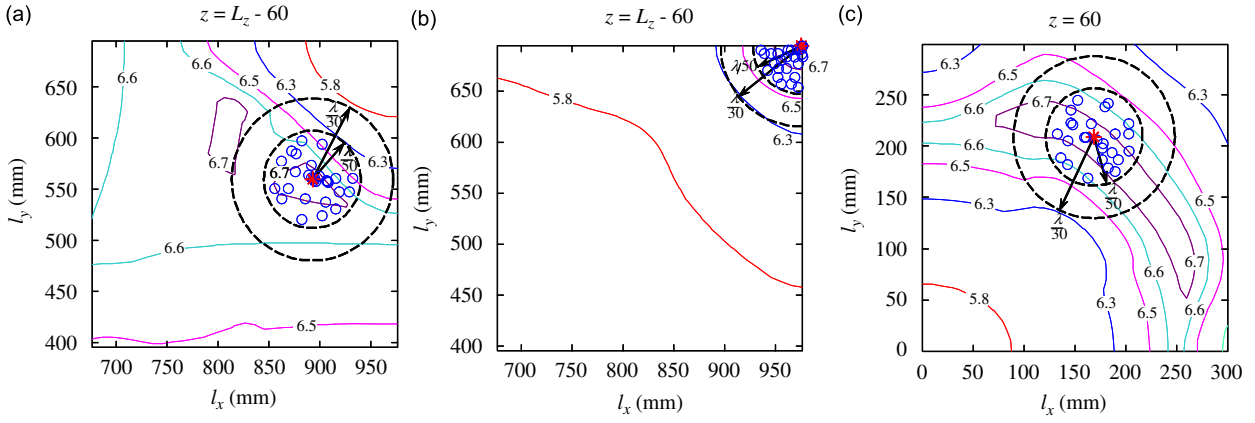

Fig. 13. Deviation criteria of the optimal locations of TARs in Surf-2 configuration: (a) deviation of TAR_145; (b) deviation of TAR_142; (c) deviation of TAR_147.

deviation between the actual SPL reductions and the optimized maximum was caped to 1 dB in the frequency band of interest. The above criterion was also tested and verified in Fig. 13 using Surf-2 configuration. Note that the location of TAR_147 is significantly different from Surf-1.

When allowing all three TARs to move around their respective optimal locations in both Surf-1 and Surf-2 configurations, it was observed that the losses in SPL reduction compared with the optimal values were caped to 0.7 and 1.1 dB within a circle of $\lambda/50$ and $\lambda/30$, respectively.

3.6. Further improvement of control effect

To further control the coupled peaks induced by TAR_142 and TAR_147, four additional TARs (TAR_138, TAR_143, TAR_146 and TAR_150) were added to the system. Because of the large number of TARs, volume searching was employed to optimize the locations of these seven TARs. Considering the practical limitation in the resonator installation already pointed out in Section 3.1, the searching space was bounded by $60.0 \leq z \leq L_z - 60.0$ mm. The optimized locations are listed in Table 6. Simulations show that a 9.3 dB reduction in the SPL was achieved, as shown in Fig. 14(a). Table 6 also shows that the optimal locations thus obtained are actually very close to the two planes with $z = 60.0$ or $L_z - 60.0$ mm. In order to accommodate experimental validation, these optimal locations were simply projected on the plane $z = 60.0$ or $L_z - 60.0$ mm to which they are close. In addition, the projected location of TAR_150 was found to be over the square hole of the loudspeaker used in experiment. To avoid interference with the loudspeaker, this resonator was moved to (13, 124, 60) mm. The distance between this location and the optimal one of TAR_150 is 37 mm, which is within the circle of $\lambda/50$. With these adjustments in the resonator locations, Fig. 14(a) shows a deterioration of 0.4 dB, among which 0.1 dB was found to be caused by the projection of the resonator locations to the two planes and 0.3 dB by the location change of TAR_150. The 0.3 dB deterioration is also consistent with the criterion established in Section 3.5.

The measured result under above modified locations of TARs is plotted in Fig. 14(b), which gave a 9.8 dB SPL reduction in the frequency band of interest. The increase of the peak value around 152 Hz due to the re-location of TAR_150 was also observed in experiment.

Table 6
Optimal locations of seven TARs targeting the peak at 145 Hz.

Optimal locations of TARs (mm)						
TAR_145	TAR_142	TAR_147	TAR_138	TAR_143	TAR_146	TAR_150
(5, 694, 79)	(967, 637, 1121)	(198, 695, 141)	(966, 690, 1101)	(971, 654, 1120)	(189, 275, 251)	(130, 87, 64)

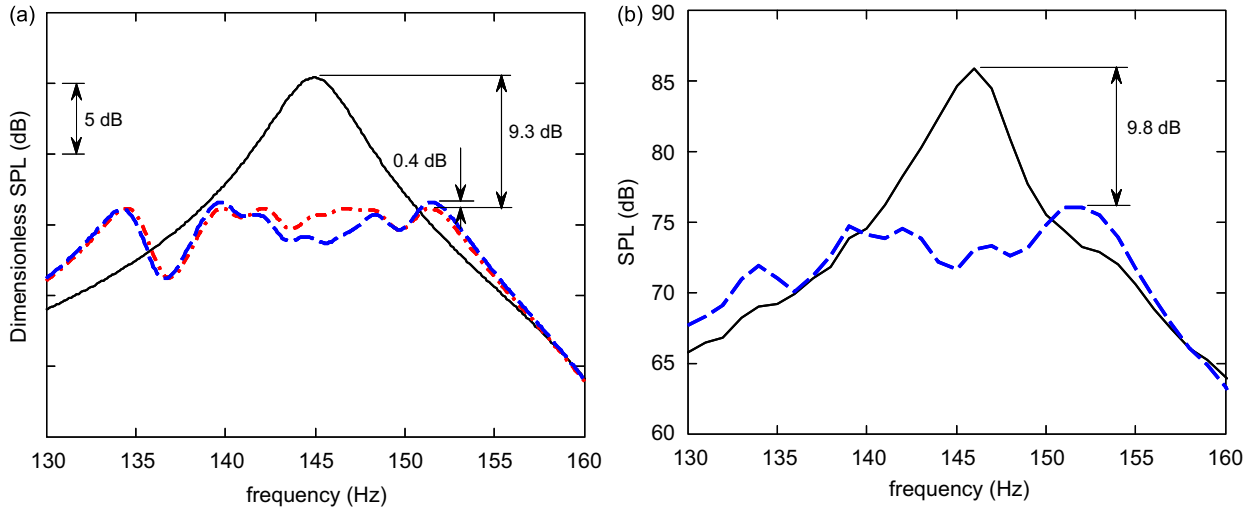

Fig. 14. Numerical and experimental comparisons on the effect of the resonator locations with seven TARs for the peak control at 145 Hz. (a) Predicted SPL curves: — without resonator; —·— with TARs at the optimal locations; —— with relocated TARs; (b) measured SPL curves: — without resonator; —— with relocated TARs.

4. Conclusions

Based on the interaction model between multiple TARs and an acoustic enclosure, the locations of a TAR array are optimized using SA approach for the reduction of the sound pressure level within a chosen band of frequency inside the acoustic enclosure. By virtue of the consideration of the full coupling between the resonators and the enclosure and among resonators themselves, the proposed approach outperforms the existing sequential design method and allows the systematic design when multiple resonators are used.

The SA searching procedure results in multiple optimal configurations for the TAR array, which ascribes to the complex enclosure–TARs interaction. Nevertheless, the control performance of TARs in terms of SPL reduction seems to be independent of the initial resonator-locations. While recognizing the physical virtue of the surface searching in handling small resonator array, volume searching shows its superiority when a large number of resonators are involved. By increasing the number of the TARs, the control performance can be significantly enhanced.

In the present configuration, the proposed deviation criteria of $\lambda/50$ and $\lambda/30$ guarantee the control performance to be within 0.5 and 1 dB of the optimized SPL reduction, respectively. As a rule of thumb, these criteria relax the restriction on the resonator installation and provide a simple guideline for the installation of TARs in practical applications. It should be cautioned, however, any generalization of these criteria to other more general cases needs more thorough and systematic investigations.

Experiments are systematically conducted to validate every major steps involved in the optimization process as well as the optimization results. Measured results agree well with numerical predictions, testifying the effectiveness and reliability of the proposed technique.

As a final note, it is relevant to mention that generic algorithm can also be used. Both GA and SA are shown to give very similar results in terms of resonator locations and control performance.

Acknowledgments

The authors wish to acknowledge a grant from Research Grants Council of Hong Kong Special Administrative Region, China (Project no. PolyU 5137/06E). Comments received from Dr. Li, Deyu during the preparation of this manuscript is also acknowledged.

References

[1] F.J. Fahy, C. Schofield, A note on the interaction between a Helmholtz resonator and an acoustic mode of an enclosure, *J. Sound Vib.* 72 (1980) 365–378.
[2] J.M. Mason, F.J. Fahy, The use of acoustically tuned resonators to improve the sound transmission loss of double-panel partitions, *J. Sound Vib.* 124 (1988) 367–379.
[3] R.A. Prydz, L.S. Wirt, H.L. Kuntz, L.D. Pope, Transmission loss of a multilayer panel with internal tuned Helmholtz resonators, *J. Acoust. Soc. Am.* 87 (1990) 1597–1602.
[4] A. Cummings, The effects of a resonator array on the sound field in a cavity, *J. Sound Vib.* 154 (1992) 25–44.
[5] S.J. Estève, M.E. Johnson, Reduction of sound transmission into a circular cylindrical shell using distributed vibration absorbers and Helmholtz resonators, *J. Acoust. Soc. Am.* 112 (2002) 2840–2848.
[6] C.Q. Howard, C.H. Hansen, A. Zander, Vibro-acoustic noise control treatments for payload bays of launch vehicles: discrete to fuzzy solutions, *Appl. Acoust.* 66 (2005) 1235–1261.
[7] D. Li, L. Cheng, Acoustically coupled model of an enclosure and a Helmholtz resonator array, *J. Sound Vib.* 305 (2007) 272–288.
[8] D. Li, J.S. Vipperman, On the design of long T-shaped acoustic resonators, *J. Acoust. Soc. Am.* 116 (2004) 2785–2792.
[9] D. Li, L. Cheng, G.H. Yu, J.S. Vipperman, Noise control in enclosures: modeling and experiments with T-shaped acoustic resonators, *J. Acoust. Soc. Am.* 122 (2007) 2615–2625.
[10] M.T. Simpson, C.H. Hansen, Use of genetic algorithms to optimize vibration actuator placement for active control of harmonic interior noise in a cylinder with floor structure, *Noise Control Eng. J.* 44 (1996) 169–184.
[11] D.S. Li, L. Cheng, C.M. Gosselin, Optimal design of PZT actuators in active structural acoustic control of a cylindrical shell with a floor partition, *J. Sound Vib.* 269 (2004) 569–588.
[12] H.Y. Guo, L. Zhang, L.L. Zhang, J.X. Zhou, Optimal placement of sensors for structural health monitoring using improved genetic algorithms, *Smart Mater. Struct.* 13 (2004) 528–534.
[13] W. Liu, W. Gao, Y. Sun, M. Xu, Optimal sensor placement for spatial lattice structure based on genetic algorithms, *J. Sound Vib.* 317 (2008) 175–189.
[14] A. Ratle, A. Berry, Use of genetic algorithms for the vibroacoustic optimization of a plate carrying point-masses, *J. Acoust. Soc. Am.* 104 (1998) 3385–3397.
[15] F.J. Fahy, *Sound and Structural Vibration: Radiation, Transmission and Response*, Academic Press, London, 1985.
[16] G. Yu, D. Li, L. Cheng, Effect of Internal resistance of a Helmholtz resonator on acoustic energy reduction in enclosures, *J. Acoust. Soc. Am.* 124 (2008) 3534–3543.
[17] S. Kirkpatrick, C.D. Gelatt Jr., M.P. Vecchi, Optimization by simulated annealing, *Science* 220 (1983) 671–680.
[18] P. Carnevali, L. Coletti, S. Patarnello, Image processing by simulated annealing, *IBM J. Res. Dev.* 29 (1985) 569–579.
[19] D. Derwent, A better way to control pollution, *Nature* 331 (1988) 575–578.
[20] I.O. Bohachevsky, M.E. Johnson, M.L. Stein, Generalized simulated annealing for function optimization, *Technometrics* 28 (1986) 209–217.
[21] D. Vanderbilt, S.G. Louie, A Monte Carlo simulated annealing approach to optimization over continuous variables, *J. Comput. Phys.* 56 (1984) 259–271.
[22] A. Corana, M. Marchesi, C. Martini, S. Ridella, Minimizing multimodal functions of continuous variables with the "simulated annealing" algorithm, *ACM Trans. Math. Software* 13 (1987) 262–280.
[23] W.L. Goffe, G.D. Ferrier, J. Rogers, Global optimization of statistical functions with simulated annealing, *J. Econometrics* 60 (1994) 65–99.
[24] X. Zha, H.V. Fuchs, C. Nocke, X. Han, Measurement of an effective absorption coefficient below 100 Hz, *Acoust. Bull.* 24 (1999) 5–10.